Journal of Materials Chemistry C

Accepted Manuscript

This article can be cited before page numbers have been issued, to do this please use: J. Ding, L. Zhao, S. Wang, S. Shao, L. Wang, X. Jing and F. Wang, *J. Mater. Chem. C*, 2015, DOI: 10.1039/C5TC01711D.

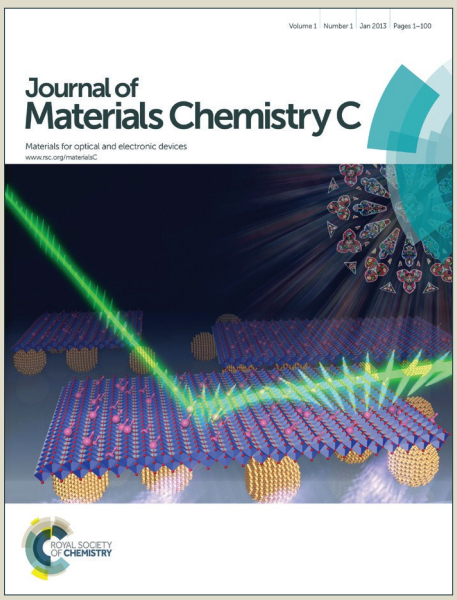

ROYAL SOCIETY OF CHEMISTRY

www.rsc.org/materialsC

View Article Online
DOI: 10.1039/C5TC01711D

Stable and Efficient Deep-Blue Terfluorenes Functionalized with Carbazole Dendrons for Solution-Processed Organic Light-Emitting Diodes

Lei Zhao,[†,‡] Shumeng Wang,[†,‡] Shiyang Shao,[†] Junqiao Ding,[*,†] Lixiang Wang,[*,†] Xiabin Jing,[†] and Fosong Wang[†]

[†]*State Key Laboratory of Polymer Physics and Chemistry, Changchun Institute of Applied Chemistry, Chinese Academy of Sciences, Changchun, 130022, P. R. China*

[‡]*University of Chinese Academy of Sciences, Beijing, 100049, P. R. China*

View Article Online
DOI: 10.1039/C5TC01711D

Abstract:

A series of solution processible deep-blue fluorescent emitters TFPC0～TFPC2 have been designed and synthesized by incorporating different generation carbazole dendrons into the 9,9-positions of the terfluorene backbone. Compared with TFPC0, the dendritic TFPC1 and TFPC2 have the elevated glass transition temperatures as well as better solubility in common organic solvents, and their high quality amorphous films can be formed via spin-coating. Noticeably, with the increasing generation number, both the intermolecular aggregate and the formation of keto defects can be effectively suppressed to avoid the appearance of the unwanted long wavelength emission. Meanwhile, the highest occupied molecular orbital (HOMO) level is gradually enhanced from TFPC0 to TFPC2, facilitating the hole injection. As a result, TFPC2 with the second generation carbazole dendrons shows the best photoluminescence and electroluminescence stability among TFPC0～TFPC2. Its corresponding solution-processed undoped device gives a state-of-art external quantum efficiency as high as 2.02% and Commission International De L'Eclairge (CIE) coordinates of (0.16, 0.04). These results indicate that the introduction of oligocarbazole is a promising strategy towards solution processible deep-blue fluorene-containing oligomers simultaneously with high spectral stability and efficiency.

View Article Online
DOI: 10.1039/C5TC01711D

Introduction

Owing to their potential applications in full-color flat-panel displays and solid-state lightings, organic light-emitting diodes (OLEDs)[1-10] have attracted much attention during the past three decades, where highly stable and luminescent materials are required to produce the three primary colors, red, green and blue. Compared with red and green counterparts, developing blue emitters remains a big challenge in terms of their inferior device efficiency, color purity and lifetime. Especially, deep-blue emitters with a Commission International De L'Eclairge (CIE) coordinate of $y < 0.10$ [11,12] are of paramount importance because the power consumption in full-color displays is dependent on the color of blue emission, that is, the smaller the CIE y value, the lower the power consumption.

Up to date, various moieties including anthracene,[13-16] pyrene,[17-19]dimesitylborane,[20] fluorene[21-26] and phenanthro[9,10-d]imidazole[27-30] have been utilized to design deep-blue fluorescent emitters. Among them, terfluorene[23,24] is believed to be a promising candidate due to its high photoluminescence quantum yield (PLQY) and wide bandgap. However, these fluorene-based derivatives may suffer from poor color purity, such as the macromolecule polyfluorene (PF). Early in 2002, E. J. W. List et al observed the appearance of a low-energy emission band at 2.2-2.3 eV corresponding to the formation of fluorenone trapping sites in the PF main chain, which turns the desired blue emission color into an undesired blue-green emission.[31] In addition, the carrier injection from the electrodes to the emitting layer (EML) seems to be problematic due to the intrinsic wide bandgap of terfluorene.[32,33] For example, there is a large hole-injection barrier of about 0.7 eV between the PEDOT:PSS modified ITO anode and the terfluorene composed EML, leading to high driving voltage as well as low device efficiency.

To overcome these problems, in this paper, we report novel stable and efficient deep-blue terfluorenes (TFPC1 and TFPC2) functionalized with different generation carbazole dendrons for solution-processed undoped OLEDs. As indicated in Figure 1, the incorporation of oligocarbazole into the 9, 9'-positions of fluorene is expected to suppress the aggregation and keto defects of the terfluorene backbone,[34] and thereby

View Article Online
DOI: 10.1039/C5TC01711D

improve the color stability. Secondly, the hole injection and transporting capability could be enhanced due to the strong electron-donating nature of oligocarbazole. Thirdly, the bulky dendrons endow these deep-blue terfluorenes with high glass transition temperature and good solubility in common organic solvents, so that high quality amorphous films can be deposited through inexpensive wet processes, such as inkjet printing and spin coating. Consequently, unlike the model compound TFPC0, TFPC2 bearing the second generation carbazole dendrons shows excellent photoluminescence (PL) and electroluminescence (EL) stability without the appearance of the green emission usually observed in fluorene-based derivatives. A peak external quantum efficiency (EQE) as high as 2.02% is simultaneously obtained together with CIE coordinates of (0.16, 0.04), which is among the highest ever reported for solution-processible undoped deep-blue fluorescent emitters.

Results and discussion

Synthesis and characterization

The synthesis of TFPC1 and TFPC2 (Scheme 1) was started from 2,7-dibromofluorenone and 2-bromofluorenone, which were arylated with aniline through electrophilic addition reaction to afford 2Br2AnF and Br2AnF. They were subsequently converted to 2Br2IF and Br2IF in 40-48% yields via a diazotization route. By using CuCl/1,10-phenanthroline as the catalyst and KOH as the base, the selective Ullmann reactions were then carried out between these iodide products and carbazole dendrons to give the key intermediates a1, a2, b1 and b2, respectively. Among them, a1 and a2 were further lithiated and converted to the corresponding trimethylene boronic esters c1 and c2. Finally, the Suzuki cross-coupling was performed to prepare the desired terfluorenes TFPC1 and TFPC2 in modest yields of 20-54%. For comparison, the model compound TFPC0 was also synthesized according to the literature method.[21] Their molecular structures were fully characterized by ^{1}H and ^{13}C NMR spectra, MALDI-TOF mass spectroscopy and elemental analysis. Moreover, with the introduction of carbazole dendrons, TFPC1 and TFPC2 are readily soluble in common organic solvents, such as chloroform,

View Article Online
DOI: 10.1039/C5TC01711D

tetrahydrofuran, toluene and chlorobenzene, ensuring their capability to form high quality films via spin-coating. This is confirmed by their atomic force microscopy (AFM) topographic images (Figure 2), where the TFPC1 and TFPC2 films displays pinhole-free and smooth surface with a root-mean-square (RMS) roughness of only 0.21-0.23 nm.

Thermal properties

The thermal properties of TFPC1 and TFPC2 together with TFPC0 were measured by thermogravimetric analysis (TGA) and differential scanning calorimetry (DSC). As presented in Figure 3, they are thermally stable with the decomposition temperatures (determined by 5% weight loss) higher than 470 ^{o}C. The glass transition temperature is found to be dependent of the generation, and increases greatly from 190 ^{o}C of TFPC0 to 304 ^{o}C of TFPC1 and 376 ^{o}C of TFPC2. Moreover, different from TFPC0 which shows a melting peak at about 373 ^{o}C, no melting process is detected for TFPC1 and TFPC2. The enhanced glass transition temperature and suppressed trend towards crystallization can be attributed to the restrained molecular movement induced by the bulky carbazole dendrons, which is beneficial for the formation of amorphous film morphology and thus the long-term operation stability of OLEDs.

Electrochemical properties:

To probe the electrochemical properties of TFPC0~TFPC2, cyclic voltammetry (CV) were performed with a three-electrode cell setup with 0.1 M n-Bu_4NClO_4 as the supporting electrolyte and ferrocene/ferrocenium(Fc/Fc^+) as the internal standard. During the anodic sweeping in dichloromethane (DCM), they all exhibit reversible oxidation processes (Figure 4). The onset potentials of TFPC0, TFPC1 and TFPC2 are observed at 0.91, 0.72 and 0.55 V, respectively. The negative shift from TFPC0 to TFPC2 is related to the increased electron-rich feature with the increasing generation number of the introduced carbazole dendrons. According to these onset potentials, the highest occupied molecular orbital (HOMO) energy levels are estimated to be -5.71

View Article Online
DOI: 10.1039/C5TC01711D

eV for TFPC0, -5.52 eV for TFPC1 and -5.35 eV for TFPC2, respectively. We note that the HOMO level of TFPC2 is much closer to the work function of PEDOT:PSS (-5.2 eV), facilitating the efficient hole injection from PEDOT:PSS to TFPC2. In contrast, no reduction processes are observed for TFPC0~TFPC2 during the cathodic scan in DCM. So their lowest unoccupied molecular orbital (LUMO) energy levels are calculated from their HOMO levels and optical bandgaps. As listed in Table 1, the LUMO levels are -2.52, -2.32 and -2.15 eV for TFPC0, TFPC1 and TFPC2, respectively.

Photophysical properties

Figure 5 shows the UV-Vis and PL spectra of TFPC0～TFPC2, and the related data are summarized in Table 1. As can be clearly seen in Figure 5a, all the emitters have a similar absorption peak at about 350 nm in toluene, corresponding to the π-π^* transition of the conjugated terfluorene backbone. But for TFPC1 and TFPC2, an additional absorption band is observed in the range of 280-320 nm, which can be safely assigned to the n-π^* and π-π^* transitions of the periphery oligocarbazole. Upon photo-excitation at 350 nm, TFPC0～TFPC2 possess strong deep-blue fluorescence in toluene with a 0-0 emission peak at about 395 nm and a 0-1 shoulder at about 414 nm. The emission profiles of TFPC1 and TFPC2 are almost the same as that of TFPC0, indicating that the structural modification at the 9-position of fluorene can barely affect the property of the lowest excited state of terfluorenes. By using 9,10-diphenylanthracene as the standard, the solution PLQYs are determined to be 88% for TFPC0, 94% for TFPC1 and 69% for TFPC2, respectively. Relative to TFPC0 and TFPC1, the lowered PLQY of TFPC2 may be tentatively ascribed to the enhanced coupling of the excited state to vibrational modes of the second generation carbazole dendron,[35] as previously observed in carbazole-based iridium dendrimers.[36]

In film state, the PL spectra of TFPC0～TFPC2 exhibit a 0-1 emission peak at about 426 nm accompanied by a 0-0 shoulder at about 407 nm (Figure 5b). Compared with the behavior in solution, the film emission maximum is red-shifted by about 30 nm, indicative of the existence of aggregation to some extent. The observation is in

View Article Online
DOI: 10.1039/C5TC01711D

agreement with the lower PLQYs (36-52%) in film than those in solution (69-94%). Despite of this, on going from TFPC0 to TFPC2, the degree of the bathochromic shift seems to be decreased, which implies that the intermolecular interactions become weakened as the dendron generation grows. This is further verified by the gradual increasing solution and film emission lifetimes from TFPC0 to TFPC2 (Table 1 and Figure S1).

To evaluate the spectral stability of these deep-blue emitters, the film PL spectra are recorded before and after annealing at 150 ^{o}C for 24 hours in air (Figure 6). As for TFPC0, a long wavelength emission occurs in the green region after annealing, whereas TFPC1 and TFPC2 show nearly unchanged PL spectra. This suggests that with the incorporation of oligocarbazole, TFPC1 and TFPC2 are more stable than TFPC0. Consistent with oligofluorenes and polyfluorenes, the improved spectral stability of TFPC1 and TFPC2 is most likely due to the reduced intermolecular aggregation as discussed above, together with the elimination of keto defects because the shielding effect from periphery dendrons can prevent oxygen from touching the 9-position carbon atom and thereby avoid its possible oxidation.

Electroluminescence properties

To investigate the EL properties of TFPC0～TFPC2, solution-processed undoped devices with a single-layer configuration of ITO/PEDOT:PSS/ TFPC0 ～ TFPC2/Ca/Al were initially fabricated, and their EL spectra are portrayed in Figure 7. As one can see, the EL spectra at a low driving voltage of 6 V for TFPC0～TFPC2 match well with their PL counterparts in solid states, giving CIE coordinates of (0.17, 0.08), (0.18, 0.06) and (0.17, 0.04). However, we note that the EL spectra significantly depend on the driving voltage. For instance, a very broad emission band in the range of 480-700 nm is observed for TFPC0 at a high driving voltage of 14 V. This unwanted emission may come from the molecular aggregation, similar to the g-band emission in polyfluorenes under electrical excitation.[37] Additionally, the contribution from the keto defects could not be excluded, for the temporal EL spectra of TFPC0 (Figure S6) show the occurrence of the green emission band peaked at around 530 nm

View Article Online
DOI: 10.1039/C5TC01711D

under aging.[31] While for TFPC1, a distinct long wavelength emission peaked at 592 nm appears when the driving voltage increases to 14 V, which is tentatively ascribed to the electromer emission.[38,39] Different from TFPC0 and TFPC1, TFPC2 displays nearly unchanged EL spectra with the increasing driving voltage. The observation demonstrates that the second generation carbazole dendron can effectively suppress the intermolecular interactions and keto defects so as to prevent the device from morphology-induced deterioration during operation.

In spite of the excellent EL stability, it should be noted that, the single-layer device performance of TFPC2 is very poor, revealing a maximum EQE of 0.11%, a maximum luminous efficiency of 0.05 cd/A and a maximum luminance of 183 cd/m^2 (Table 2 and Figure S3-S5). Therefore, a double-layer device is then prepared for TFPC2 with a structure of ITO/PEDOT:PSS/TFPC2/TPBI/LiF/Al, where TPBI (1,3,5-tris(1-phenyl-benzimidazole-2-yl)benzene) acts as the electron transporting layer. As indicated in Figure 8, a state-of-art EQE as high as 2.02% is achieved together with a maximum luminous efficiency of 0.86 cd/A and a maximum luminance of 1054 cd/m^2. The EQE is enhanced by about 20 times compared with the single-layer device because the insertion of an additional TPBI layer could improve the electron injection/transporting and lead to more balanced charge flux. Most importantly, similar to the single-layer device, the EL spectrum of TFPC2 is independent of the driving voltage. As a consequence, a very stable deep-blue emission is realized with CIE coordinates of (0.16, 0.04), close to the National Television System Committee (NTSC) standard blue value of (0.14, 0.08) or the European Broadcasting Union (EBU) one of (0.15, 0.06). Given the efficiency and color purity, to the best of our knowledge, TFPC2 is among the most promising deep-blue fluorescent emitters used for solution-processed undoped OLEDs.

Conclusion

In conclusion, we have designed and synthesized a series of solution processible deep-blue fluorescent emitters TFPC0～TFPC2 by functionalizing the terfluorene backbone with different generation carbazole dendrons. The introduction of the bulky

View Article Online
DOI: 10.1039/C5TC01711D

hole-transporting oilgocarbazole, it is found that, can improve the thermal stability and solution processibility to ensure the formation of high quality amorphous films, suppress the aggregate and keto defects to avoid the unwanted long wavelength emission usually observed in fluorene derivatives, and elevate the HOMO level to facilitate the hole injection. Consequently, a very stable and highly efficient deep-blue emission is achieved for TFPC2 bearing the second generation carbazole dendrons, which shows a promising EQE of 2.02% with CIE coordinates of (0.16, 0.04). We believe that this work will pave the way to the development of high performance oligofluorene-based deep-blue emitters used for solution-processed undoped OLEDs.

Experimental section

General information

^{1}H and ^{13}C NMR spectra were recorded with a Bruker Avance 300 NMR spectrometer. Elemental analyses of carbon, hydrogen, and nitrogen were performed on a VarioEL elemental analyzer. MALDI/TOF mass spectra were obtained on an AXIMA CFR MS apparatus (COMPACT). Thermal gravimetric analysis (TGA) and differential scanning calorimetry (DSC) were performed on Perkin Elmer-TGA 7 and Perkin Elmer-DSC 7 system under nitrogen at a heating rate of 10 ^{o}C min^{-1}. The UV/visible absorption and photoluminescent spectra were measured by a Perkin-Elmer Lambda 35 UV/vis spectrometer and a Perkin-Elmer LS 50B spectrofluorometer, respectively. The PL quantum yields of the terfluorenes in toluene solution were measured by excitation at 350 nm with 9,10-diphenylanthracene (ca. 5 $\times$ 10^{-6} M solution in cyclohexane, PLQY = 0.9) as the standard. Thin films for spectroscopic measurements were prepared by spin-coating on quartz. The quantum efficiencies of the solid films were recorded by measuring the total light output in all directions in an integrating sphere (C9920-02, HAMAMATSU). Emission lifetimes were obtained by double exponential fit of emission decay curves recorded on a system equiped with a Quanty-ray FLS920 pulsed Ti:Saph laser with THG 376 nm output and ca. 20 ps pulse width. Cyclic voltammetry (CV) measurements were obtained in anhydrous dichloromethane with Bu_4NClO_4 (0.1 mol L^{-1}) as the

View Article Online
DOI: 10.1039/C5TC01711D

electrolyte on a CHI660a electrochemical analyzer under a scan rate of 100 mV s^{-1}. A glass carbon electrode, a Ag/AgCl electrode and a Pt wire were used as the working electrode, the reference electrode and the counter electrode, respectively.

Device fabrication and measurement

Patterned glass substrates coated with indium tin oxide (ITO) (20 Ω per square) were cleaned with acetone, detergent, and distilled water and then were cleaned in an ultrasonic solvent bath. After baking in a heating chamber at 120 °C for 8 h, the ITO-glass substrates were treated with O_2 plasma for 30 min. Subsequently, poly(3,4-ethylenedioxythiophene):poly(styrenesulfonate) (PEDOT:PSS, Batron-P4083, Bayer AG) was spin-coated on top of the ITO at a speed of 5000 rpm for 60 s and then baked at 120 °C for 45 min. Then, solutions of the emitters (10 mg/mL) in *o*-dichlorobenzene were filtered through a filter (0.45 μm) and spin-coated on PEDOT:PSS as the emissive layer (EML) at a speed of 1500 rpm for 60 s. Successively, the substrate was annealed at 100 °C for 30 min inside a nitrogen-filled glovebox and then transferred to a vacuum thermal evaporator. On top of the EML, calcium was thermally deposited through a shadow mask with an array of 70 mm^2 openings at a pressure of 4.0×10^{-4} Pa. Finally, aluminum was deposited subsequently as the protective layer for calcium. For the bilayer device, a 50 nm-thick TPBI film was evaporated on top of the EML, and then 1 nm LiF and 100 nm Al were deposited subsequently as the cathode. The EL spectra and CIE coordinates were measured using a PR650 spectra colorimeter. The current−voltage and brightness−voltage curves of devices were measured using a Keithley 2400/2000 source meter and a calibrated silicon photodiode. All the measurements were carried out at room temperature under ambient conditions.

Synthesis:

All solvents for chemical synthesis were refined according to the standard procedures. 2,7-dibromofluorenone, 2-bromofluorenone, 3,6-di-*tert*-butyl-carbazole and 3,6-bis(3,6-di-*tert*-butylcarbazol-9-yl)-carbazole were prepared according to

View Article Online
DOI: 10.1039/C5TC01711D

literature methods. [40-42]

4-(9-(4-aminophenyl)-2,7-dibromofluoren-9-yl)benzenamine (2Br2AnF): 2,7-Dibromofluorenone (3.38 g, 10 mmol), aniline (13.96 g, 150 mmol), methylsulphonic acid (0.64 mL, 10 mmol) were mixed in a three-necked round-bottom flask and refluxed for 6 hours at 150 ^{o}C under N_2 atmosphere. After cooling to room temperature, 100 mL water was added to the solution. The mixture was filtered and the residue was washed with water. The residue was recrystallized from ethanol to give the product as a gray solid in 67% yield. ^{1}H NMR (300 MHz, $CDCl_3$) δ 7.55 (d, J = 7.8 Hz, 2H), 7.42 (m, 4H), 6.93 (d, J = 7.8 Hz, 4H), 6.56 (d, J = 8.7 Hz, 4H), 3.62 (s, 4H).

2,7-dibromo-9,9-bis(4-iodophenyl)fluorene (2Br2IF):

2Br2AnF (2.03 g, 4.0 mmol), hydrochloric acid (1.33 mL, 16 mmol) and H_2O (20 mL) were mixed in a flask and were cooled to 0 ^{o}C. Sodium nitrite (0.56 g, 8.0 mmol) and H_2O (2 mL) were then slowly added. After stirring for 30 minute, a solution of KI (1.46 g, 8.8 mmol) in 5 mL H_2O was added into the mixture at 0 ^{o}C. After aging for 1 hour, the mixture was heated at 80 ^{o}C overnight. The mixture was filtered and the residue was washed with water. The crude product was purified by column chromatography on silica gel with petroleum ether as eluent to give a white solid in 40% yield. ^{1}H NMR (300 MHz, $CDCl_3$) δ 7.59 (m, 6H), 7.51 (dd, J = 8.2, 1.5 Hz, 2H), 7.41 (d, J = 1.5 Hz, 2H), 6.87 (d, J = 8.7 Hz, 4H).

4-(9-(4-aminophenyl)-2-bromofluoren-9-yl)benzenamine (Br2AnF):

Br2AnF was prepared in 72% yield according to a similar procedure to 2Br2AnF by using 2-bromofluoren-9-one instead of 2,7-dibromofluoren-9-one. ^{1}H NMR (300 MHz, $CDCl_3$) δ 7.53 (d, J = 7.8 Hz, 1H), 7.492 (d, J = 8.1 Hz, 1H), 7.47 – 7.43 (m, 4H), 7.42 – 7.36 (m, 1H), 7.33 (d, J = 1.6 Hz, 1H), 7.21 (ddd, J = 10.9, 6.0, 3.4 Hz, 1H), 7.17 – 7.14 (m, 2H), 6.93 – 6.85 (m, 4H), 3.63 (s, 4H).

2-bromo-9,9-bis(4-iodophenyl)-fluorene (Br2IF):

Br2IF was prepared from Br2AnF in 48% yield according to the procedure similar to Br2IF. ^{1}H NMR (300 MHz, $CDCl_3$) δ 7.73 (d, J = 7.5 Hz, 1H), 7.62 (d, J = 8.1 Hz, 1H), 7.59 – 7.52 (m, 4H), 7.52 – 7.46 (m, 1H), 7.43 (d, J = 1.6 Hz, 1H), 7.37 (ddd, J =

View Article Online
DOI: 10.1039/C5TC01711D

10.9, 6.0, 3.4 Hz, 1H), 7.32 – 7.27 (m, 2H), 6.93 – 6.85 (m, 4H).

2,7-dibromo-9,9-bis[4-(3,6-di-*tert*-butylcarbazol-9-yl)phenyl]fluorene (a1):

2Br2IF (2.10 g, 3.0 mmol) and 3,6-di-tert-butyl-carbazole (1.70 g, 6.3 mmol,), CuCl (0.11 g, 1.2 mmol), KOH (1.02 g, 18 mmol) , 1,10-phenanthroline monohydrate (0.23 g, 1.2 mmol) and xylene (20 mL) were added into around-bottom flask and refluxed for 24 hours at 150 ^{o}C under N_2 atmosphere. After cooling to room temperature, the reaction mixture was extracted with CH_2Cl_2 (50 mL × 2). The combined organic phase was washed with water, dried over anhydrous Na_2SO_4, filtered and the solvent was removed in a vacuum. The crude product was purified by column chromatography over silica gel eluting with a mixture of CH_2Cl_2/hexane (1/4) to give a white solid in 50% yield. ^{1}H NMR (300 MHz, $CDCl_3$) δ 8.13 (d, *J* = 1.5 Hz, 4H), 7.74 – 7.66 (m, 4H), 7.59 (dd, *J* = 8.2, 1.6 Hz, 2H), 7.52 (d, *J* = 8.6 Hz, 4H), 7.49 – 7.37 (m, 12H), 1.46 (s, 36H).

2,7-dibromo-9,9-bis{4-[3,6-bis

(3,6-di-*tert*-butylcarbazol-9-yl)carbazole-9-yl]phenyl}fluorene (a2):

a2 was prepared in 21% yield according to a similar procedure to a1 by using 3,6-bis(3,6-di-tert-butylcarbazol-9-yl)-carbazole instead of 3,6-di-*tert*-butyl-carbazole. ^{1}H NMR (300 MHz, $CDCl_3$) δ 8.24 (d, *J* = 1.8 Hz, 4H), 8.16 (d, *J* = 1.6 Hz, 8H), 7.81 – 7.74 (m, 4H), 7.74 – 7.69 (m, 6H), 7.67 – 7.57 (m, 12H), 7.46 (dd, *J* = 8.7, 1.8 Hz, 8H), 7.34 (d, *J* = 8.6 Hz, 8H), 1.46 (s, 72H).

2-bromo-9,9-bis[4-(3,6-di-*tert*-butylcarbazol-9-yl)phenyl]fluorene (b1):

b1 was prepared in 48% yield according to a similar procedure to a1 by using Br2IF instead of 2Br2IF. ^{1}H NMR (300 MHz, $CDCl_3$) δ 8.12 (s, 4H), 7.82 (d, *J* = 7.4 Hz, 1H), 7.76 – 7.67 (m, 2H), 7.58 (d, *J* = 8.3 Hz, 2H), 7.53 – 7.33 (m, 18H), 1.45 (s, 36H).

2-bromo-9,9-bis{4-[3,6-bis

(3,6-di-*tert*-butylcarbazol-9-yl)carbazole-9-yl]phenyl}fluorene (b2): b2 was prepared in 29% yield according to a similar procedure to a1 by using Br2IF instead of 2Br2IF and 3,6-bis(3,6-di-*tert*-butylcarbazol-9-yl)-carbazole instead of 3,6-di-*tert*-butyl-carbazole. ^{1}H NMR (300 MHz, $CDCl_3$) δ 8.23 (d, *J* = 1.7 Hz, 4H),

View Article Online
DOI: 10.1039/C5TC01711D

8.15 (d, *J* = 1.7 Hz, 8H), 7.89 (dd, *J* = 6.3, 2.2 Hz, 1H), 7.80 (dd, *J* = 7.7, 4.9 Hz, 2H), 7.75 – 7.64 (m, 12H), 7.64 – 7.56 (m, 5H), 7.54 – 7.48 (m, 2H), 7.45 (dd, *J* = 8.7, 1.9 Hz, 8H), 7.32 (d, *J* = 8.6 Hz, 8H), 1.46 (s, 72H).

9,9-bis[4-(3,6-di-*tert*-butylcarbazol-9-yl)phenyl]fluorine-2,7-bis(trimethylene boronate) (c1):

Compound a1 (0.93 g, 0.5 mmol) was disolved in dry tetrahydrofuran (30 mL) under argon and cooled to -78 ^{o}C. Then *n*-butyl lithium (0.52 mL, 1.3 mmol) was slowly added under vigorous stirring. After stirring for 2 hours, triethyl borate (0.17 mL, 1.5 mmol) was added and the mixture was stirred for another 8 hours at -78 ^{o}C. Subsequently the mixture was warmed to room temperature and poured into 2 N HCl aqueous. The mixture was extracted with ether, washed with brine and dried over anhydrous Na_2SO_4. The extract was evaporated to dryness affording a yellow solid. This solid was then dissolved in 30 mL toluene and 1,3-propylenediol (0.45 g, 5 mmol). The mixture was stirred at 110 ^{o}C under argon for 8 hours. After cooling to room temperature, the mixture was extracted with ether, washed with brine and dried over anhydrous Na_2SO_4. The extract was evaporated to dryness to afford the crude product as a yellow solid, which was further purified by column chromatography over silica gel with CH_2Cl_2/hexane (1/4) as the eluent to give a white solid in 56% yield. ^{1}H NMR (300 MHz, $CDCl_3$) δ 8.12 (d, *J* = 1.3 Hz, 4H), 7.95 (s, 2H), 7.91 – 7.83 (m, 4H), 7.45 (ddd, *J* = 18.6, 14.9, 8.6 Hz, 16H), 4.17 (t, *J* = 5.2 Hz, 8H), 2.14 – 2.02 (m, 4H), 1.45 (s, 36H).

9,9-bis{4-[3,6-bis (3,6-di-*tert*-butylcarbazol-9-yl)carbazole-9-yl]phenyl}fluorene -2,7-bis(trimethylene boronate) (c2):

Compound c2 was prepared from a2 in 44% yield according to the procedure similar to c1. ^{1}H NMR (300 MHz, $CDCl_3$) δ 8.22 (d, *J* = 1.8 Hz, 4H), 8.15 (d, *J* = 1.7 Hz, 8H), 8.05 (s, 2H), 7.92 (q, *J* = 7.7 Hz, 4H), 7.75 – 7.63 (m, 12H), 7.60 (dd, *J* = 8.7, 1.8 Hz, 4H), 7.45 (dd, *J* = 8.7, 1.8 Hz, 8H), 7.33 (d, *J* = 8.6 Hz, 8H), 4.19 (t, *J* = 5.1 Hz, 8H), 2.14 – 2.02 (m, 4H), 1.44 (s, 72H).

TFPC1:

Compound c1 (0.52 g, 0.5 mmol), b1 (1.04 g, 1.1 mmol) and $Pd(PPh_3)_4$ (12 mg, 0.01

View Article Online
DOI: 10.1039/C5TC01711D

mmol) were dissolved in 30 mL toluene. An aqueous solution of 2 M K_2CO_3 (1 mL, 2.0 mmol) and one drop of Aliquat 336 was added to the solution and then the mixture was heated to 100 ^oC for 12 hours under argon. After reaction, 50 mL CH_2Cl_2 was added to the solution. The organic phase was washed with water and dried with anhydrous Na_2SO_4. Solvents were removed under vacuum and the residue was purified by column chromatography over silica gel with CH_2Cl_2/hexane (1/2) as the eluent to give the product as a white solid in 54% yield. ^1H NMR (300 MHz, $CDCl_3$) δ 8.06 (d, *J* = 8.6 Hz, 12H), 7.95 (dd, *J* = 7.9, 5.1 Hz, 5H), 7.89 (d, *J* = 6.3 Hz, 6H), 7.76 (d, *J* = 7.9 Hz, 4H), 7.62 (d, *J* = 8.3 Hz, 7H), 7.56 (d, *J* = 8.6 Hz, 9H), 7.52 – 7.45 (m, 14H), 7.43 (d, *J* = 7.6 Hz, 3H), 7.38 – 7.28 (m, 17H), 7.24 (s, 3H), 1.37 (d, *J* = 13.3 Hz, 108H). ^{13}C NMR (300 MHz, $CDCl_3$) δ151.93, 151.67, 151.17, 144.19, 144.12, 142.81, 141.05, 140.89, 139.77, 139.23, 139.11, 137.23, 137.10, 129.48, 128.04, 127.23, 126.67, 124.93, 123.53, 123.36, 120.83, 120.60, 116.15, 109.23, 65.25, 34.66, 34.62, 31.96. MS (MALDI-TOF) m/z: 2613.48 [M^+]. Anal. Calcd for $C_{195}H_{188}N_6$: C, 89.54; H, 7.24; N, 3.21. Found: C, 89.60; H, 7.21; N, 3.16.

TFPC2:

TFPC2 was prepared from c2 and b2 in 20% yield according to the procedure similar to TFPC1. ^1H NMR (300 MHz, $CDCl_3$) δ 8.13 (dd, *J* = 14.0, 1.5 Hz, 26H), 8.09 – 7.99 (m, 18H), 7.93 (dd, *J* = 12.4, 7.5 Hz, 6H), 7.80 (d, *J* = 8.5 Hz, 4H), 7.73 (d, *J* = 8.6 Hz, 8H), 7.62 (q, *J* = 8.5 Hz, 24H), 7.54 – 7.47 (m, 12H), 7.43 (dd, *J* = 8.8, 1.7 Hz, 5H), 7.40 – 7.29 (m, 18H), 7.29 – 7.20 (m, 23H), 7.17 (d, *J* = 8.6 Hz, 8H), 1.38 (d, *J* = 11.0 Hz, 216H). ^{13}C NMR (300 MHz, $CDCl_3$) δ151.55, 151.35, 150.78, 145.43, 142.52, 140.99, 140.60, 140.24, 140.15, 140.03, 139.97, 139.67, 139.37, 137.83, 136.56, 136.36, 130.96, 129.92, 129.02, 128.21, 127.50, 127.25, 125.84, 125.29, 124.04, 123.47, 123.09, 123.05, 119.31, 116.16, 111.03, 109.04, 65.37, 34.54, 32.00. MS (MALDI-TOF) m/z: 5271.16 [M^+]. Anal. Calcd for $C_{387}H_{368}N_{18}$: C, 88.18; H, 7.04; N, 4.78. Found: C, 88.32; H, 6.96; N, 4.96.

Acknowledgements

The authors are grateful to the 973 Project (No. 2015CB655001) and Natural Science

View Article Online
DOI: 10.1039/C5TC01711D

Foundation of China (Nos 21174144, 51322308 and 91333205) for financial support of this research.

References

1 C. W. Tang and S. A. Vanslyke, *Appl Phys Lett*, 1987, **51**, 913-915.
2 M. A. Baldo, M. E. Thompson and S. R. Forrest, *Nature*, 2000, **403**, 750-753.
3 B. W. D'Andrade and S. R. Forrest, *Adv Mater*, 2004, **16**, 1585-1595.
4 C. C. Wu, Y. T. Lin, K. T. Wong, R. T. Chen and Y. Y. Chien, *Adv Mater*, 2004, **16**, 61-65.
5 S. J. Su, E. Gonmori, H. Sasabe and J. Kido, *Adv Mater*, 2008, **20**, 4189-4194
6 Z. Q. Jiang, Z. Y. Liu, C. L. Yang, C. Zhong, J. G. Qin, G. Yu and Y. Q. Liu, *Adv Funct Mater*, 2009, **19**, 3987-3995.
7 K. T. Kamtekar, A. P. Monkman and M. R. Bryce, *Adv Mater*, 2010, **22**, 572-582.
8 M. R. Zhu, Q. A. Wang, Y. Gu, X. S. Cao, C. Zhong, D. G. Ma, J. G. Qin and C. L. Yang, *J Mater Chem*, 2011, **21**, 6409-6415.
9 G. X. Jiang, C. L. Bian, J. Q. Ding and L. X. Wang, *Chinese J Polym Sci*, 2013, **31**, 787-797.
10 D. B. Xia, B. Wang, B. Chen, S. M. Wang, B. H. Zhang, J. Q. Ding, L. X. Wang, X. B. Jing and F. S. Wang, *Angew Chem Int Edit*, 2014, **53**, 1048-1052.
11 B. Chen, J. Q. Ding, L. X. Wang, X. B. Jing and F. S. Wang, *Chem Commun*, 2012, **48**, 8970-8972.
12 M. Q. Yu, S. M. Wang, S. Y. Shao, J. Q. Ding, L. X. Wang, X. B. Jing and F. S. Wang, *J Mater Chem C*, 2015, **3**, 861-869.
13 C. Adachi, T. Tsutsui and S. Saito, *Appl Phys Lett*, 1990, **56**, 799-801.
14 R. Kim, S. Lee, K. H. Kim, Y. J. Lee, S. K. Kwon, J. J. Kim and Y. H. Kim, *Chem Commun*, 2013, **49**, 4664-4666.
15 H. Park, J. Lee, I. Kang, H. Y. Chu, J. I. Lee, S. K. Kwon and Y. H. Kim, *J Mater Chem*, 2012, **22**, 2695-2700.
16 Z. Q. Wang, C. Xu, W. Z. Wang, L. M. Duan, Z. Li, B. T. Zhao and B. M. Ji, *New J Chem*, 2012, **36**, 662-667.
17 G. Mallesham, C. Swetha, S. Niveditha, M. E. Mohanty, N. J. Babu, A. Kumar, K. Bhanuprakash and V. J. Rao, *J Mater Chem C*, 2015, **3**, 1208-1224.
18 F. Liu, W. Y. Lai, C. Tang, H. B. Wu, Q. Q. Chen, B. Peng, W. Wei, W. Huang and Y. Cao, *Macromol Rapid Comm*, 2008, **29**, 659-664.
19 J. You, G. Y. Li, R. J. Wang, Q. P. Nie, Z. G. Wang and J. Y. Li, *Phys Chem Chem Phys*, 2011, **13**, 17825-17830.
20 S. L. Lin, L. H. Chan, R. H. Lee, M. Y. Yen, W. J. Kuo, C. T. Chen and R. J.

View Article Online
DOI: 10.1039/C5TC01711D

Jeng, *Adv Mater*, 2008, **20**, 3947-3952.

21 K. T. Wong, Y. Y. Chien, R. T. Chen, C. F. Wang, Y. T. Lin, H. H. Chiang, P. Y. Hsieh, C. C. Wu, C. H. Chou, Y. O. Su, G. H. Lee and S. M. Peng, *J Am Chem Soc*, 2002, **124**, 11576-11577.

22 S. Tang, M. Liu, P. Lu, H. Xia, M. Li, Z. Q. Xie, T. Z. Shen, C. Gu, H. P. Wang, B. Yang and Y. G. Ma, *Adv Funct Mater*, 2007, **17**, 2869-2877.

23 C. G. Zhen, Y. F. Dai, W. J. Zeng, Z. Ma, Z. K. Chen and J. Kieffer, *Adv Funct Mater*, 2011, **21**, 699-707.

24 C. G. Zhen, Z. K. Chen, Q. D. Liu, Y. F. Dai, R. Y. C. Shin, S. Y. Chang and J. Kieffer, *Adv Mater*, 2009, **21**, 2425-2429.

25 X. C. Wang, L. Zhao, S. Y. Shao, J. Q. Ding, L. X. Wang, X. B. Jing and F. S. Wang, *Polymer Chemistry*, 2014, **5**, 6444-6451.

26 X. C. Wang, L. Zhao, S. Y. Shao, J. Q. Ding, L. X. Wang, X. B. Jing and F. S. Wang, *Macromolecules*, 2014, **47**, 2907-2914.

27 C. J. Kuo, T. Y. Li, C. C. Lien, C. H. Liu, F. I. Wu and M. J. Huang, *J Mater Chem*, 2009, **19**, 1865-1871.

28 W. J. Li, D. D. Liu, F. Z. Shen, D. G. Ma, Z. M. Wang, T. Feng, Y. X. Xu, B. Yang and Y. G. Ma, *Adv Funct Mater*, 2012, **22**, 2797-2803.

29 Y. Zhang, S. L. Lai, Q. X. Tong, M. F. Lo, T. W. Ng, M. Y. Chan, Z. C. Wen, J. He, K. S. Jeff, X. L. Tang, W. M. Liu, C. C. Ko, P. F. Wang and C. S. Lee, *Chem Mater*, 2012, **24**, 61-70.

30 S. T. Zhang, W. J. Li, L. Yao, Y. Y. Pan, F. Z. Shen, R. Xiao, B. Yang and Y. G. Ma, *Chem Commun*, 2013, **49**, 11302-11304.

31 E. J. W. List, R. Guentner, P. S. de Freitas and U. Scherf, *Adv Mater*, 2002, **14**, 374-378.

32 C. Ego, A. C. Grimsdale, F. Uckert, G. Yu, G. Srdanov and K. Mullen, *Adv Mater*, 2002, **14**, 809-811.

33 Z. Q. Gao, Z. H. Li, P. F. Xia, M. S. Wong, K. W. Cheah and C. H. Chen, *Adv Funct Mater*, 2007, **17**, 3194-3199.

34 S. Setayesh, A. C. Grimsdale, T. Weil, V. Enkelmann, K. Mullen, F. Meghdadi, E. J. W. List and G. Leising, *J Am Chem Soc*, 2001, **123**, 946-953.

35 D. Phillips, *J. Photochem. Photobiol. A*, 1997, **105**, 307-315.

36 K. A. Knights, S. G. Stevenson, C. P. Shipley, S. –C. Lo, S. Olsen, R. E. Harding, S. Gambino, P. L. Burn, I. D. W. Samuel, *J. Mater. Chem.*, 2008, **18**, 2121-2130.

37 R. Grisorio, G. Allegretta, P. Mastrorilli and G. P. Suranna, *Macromolecules*, 2011, **44**, 7977-7986.

38 J. Kalinowski, G. Giro, M. Cocchi, V. Fattori and P. Di Marco, *Appl Phys Lett*, 2000, **76**, 2352-2354.

39 J. Y. Hu, Y. J. Pu, Y. Yamashita, F. Satoh, S. Kawata, H. Katagiri, H. Sasabe and J. Kido, *J Mater Chem C*, 2013, **1**, 3871-3878.

40 J. Q. Ding, J. H. Lu, Y. X. Cheng, Z. Y. Xie, L. X. Wang, X. B. Jing and F. S.

View Article Online
DOI: 10.1039/C5TC01711D

Wang, *Adv Funct Mater*, 2008, **18**, 2754-2762.

41 P. Moonsin, N. Prachumrak, R. Rattanawan, T. Keawin, S. Jungsuttiwong, T. Sudyoadsuk and V. Promarak, *Chem Commun*, 2012, **48**, 3382-3384.

42 X. D. Wang, S. M. Wang, Z. H. Ma, J. Q. Ding, L. X. Wang, X. B. Jing and F. S. Wang, *Adv Funct Mater*, 2014, **24**, 3413-3421.

View Article Online
DOI: 10.1039/C5TC01711D

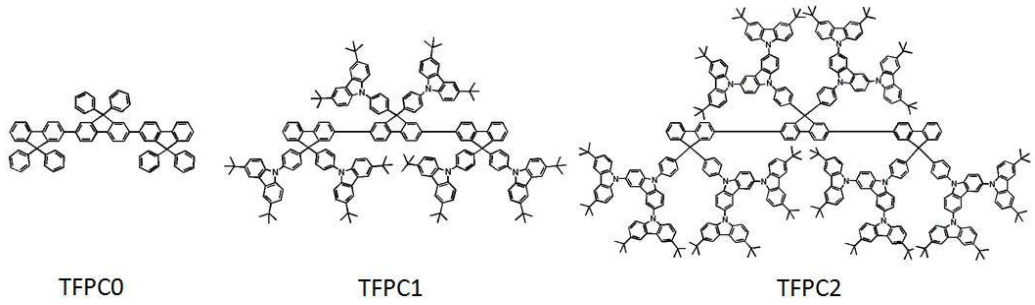

Figure 1. Molecular structures of TFPC0~TFPC2

Scheme 1. Sythesis of TFPC1 and TFPC2.

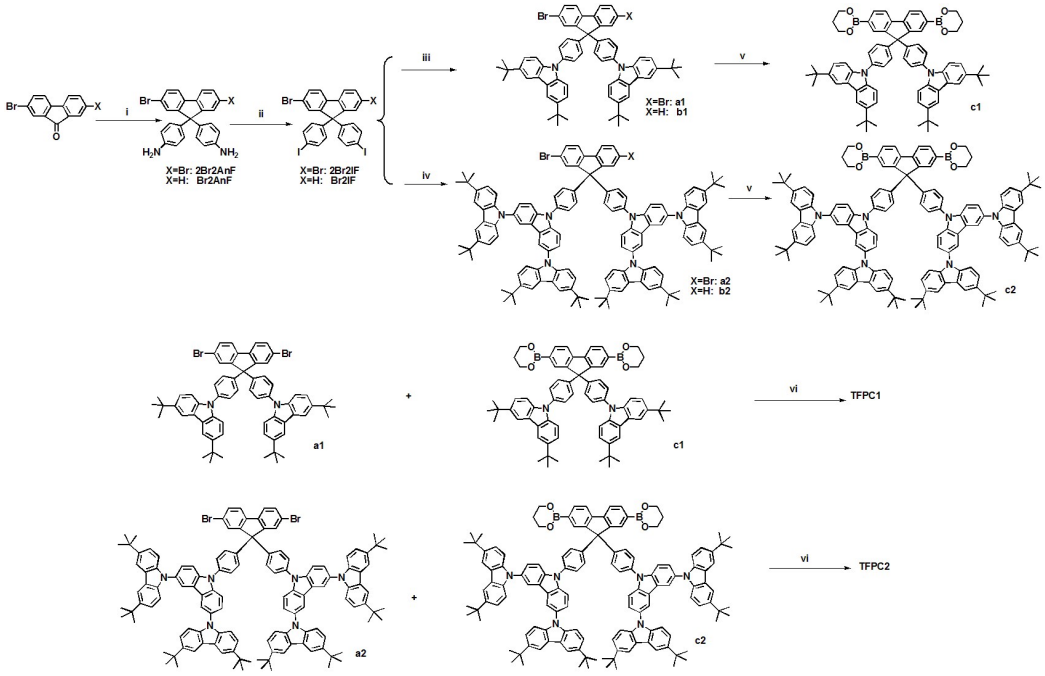

Reagents and conditions: (i) aniline, CH_3SO_3H, 130 ^oC; (ii) HCl, $NaNO_2$, KI; (iii) KOH, CuCl, 1,10-phenanthroline ,3,6-di-*tert*-butyl-carbazole, xylene, 140 ^oC; (iv) KOH, CuCl, 1,10-phenanthroline, 3,6-bis(3,6-di-*tert*-butylcarbazol-9-yl)-carbazole, xylene, 140 ^oC ; (v) *n*-C_4H_9Li, $B(OCH)_3$, THF, then H^+; (vi) $Pd(PPh_3)_4$, 2 M K_2CO_3, Aliquat 336, toulene, 100 ^oC.

View Article Online
DOI: 10.1039/C5TC01711D

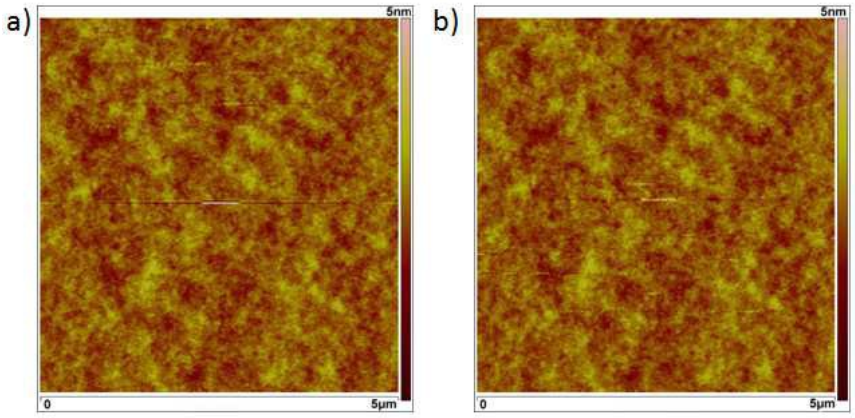

Figure 2. AFM images of the TFPC1 (a) and TFPC2 (b) films prepared through spin-coating from chlorobenzene solutions at a concentration of 10 mg/mL Surface roughness amplitude: (a) 0.23 nm; (b) 0.21 nm.

View Article Online
DOI: 10.1039/C5TC01711D

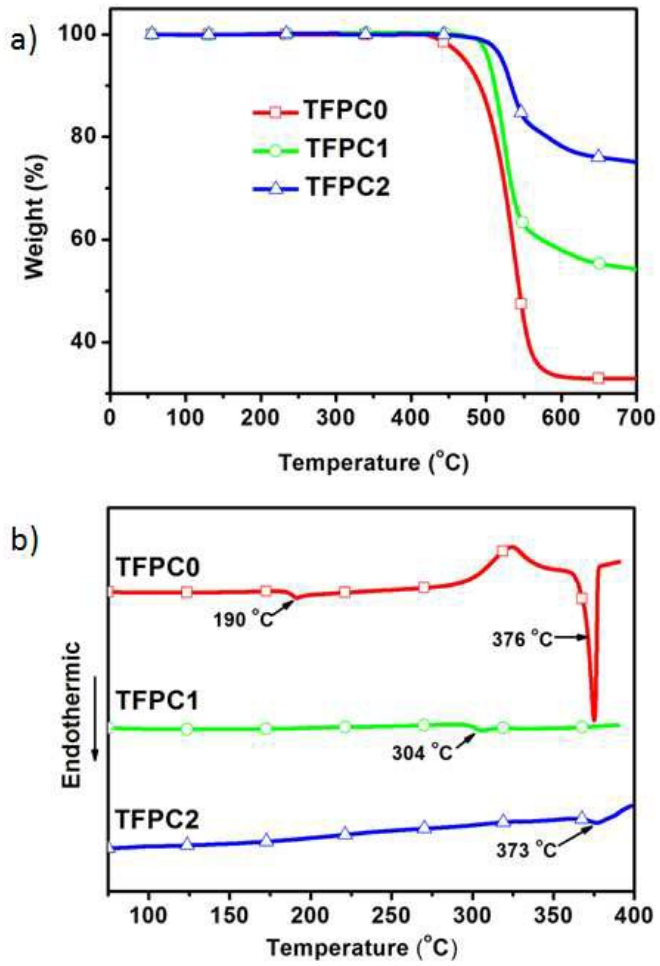

Figure 3. TGA (a) and DSC (b) traces of TFPC0~TFPC2 measured at a heating rate of 10 ^{o}C min^{-1} under N_2.

View Article Online
DOI: 10.1039/C5TC01711D

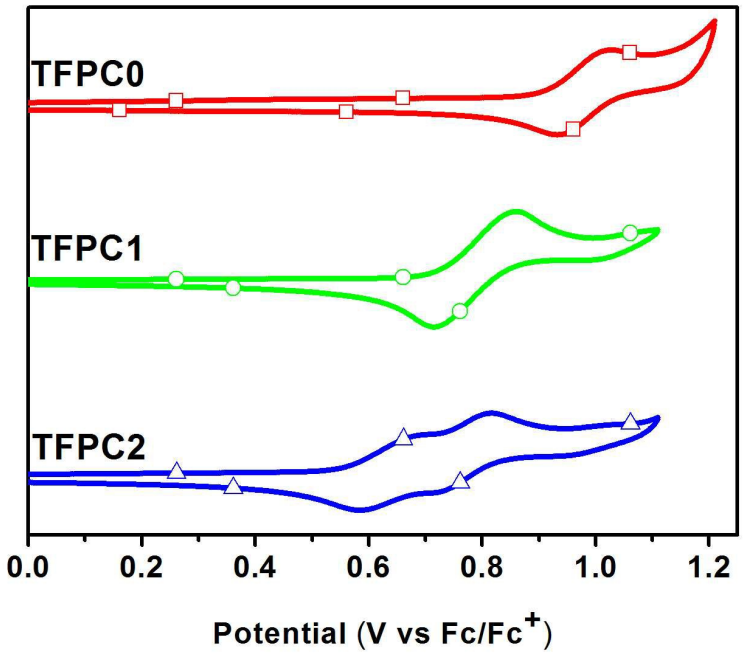

Figure 4. Cyclic voltammograms of TFPC0~TFPC2 measured in CH_2Cl_2 under a scan rate of 100 mV s^{-1}.

View Article Online
DOI: 10.1039/C5TC01711D

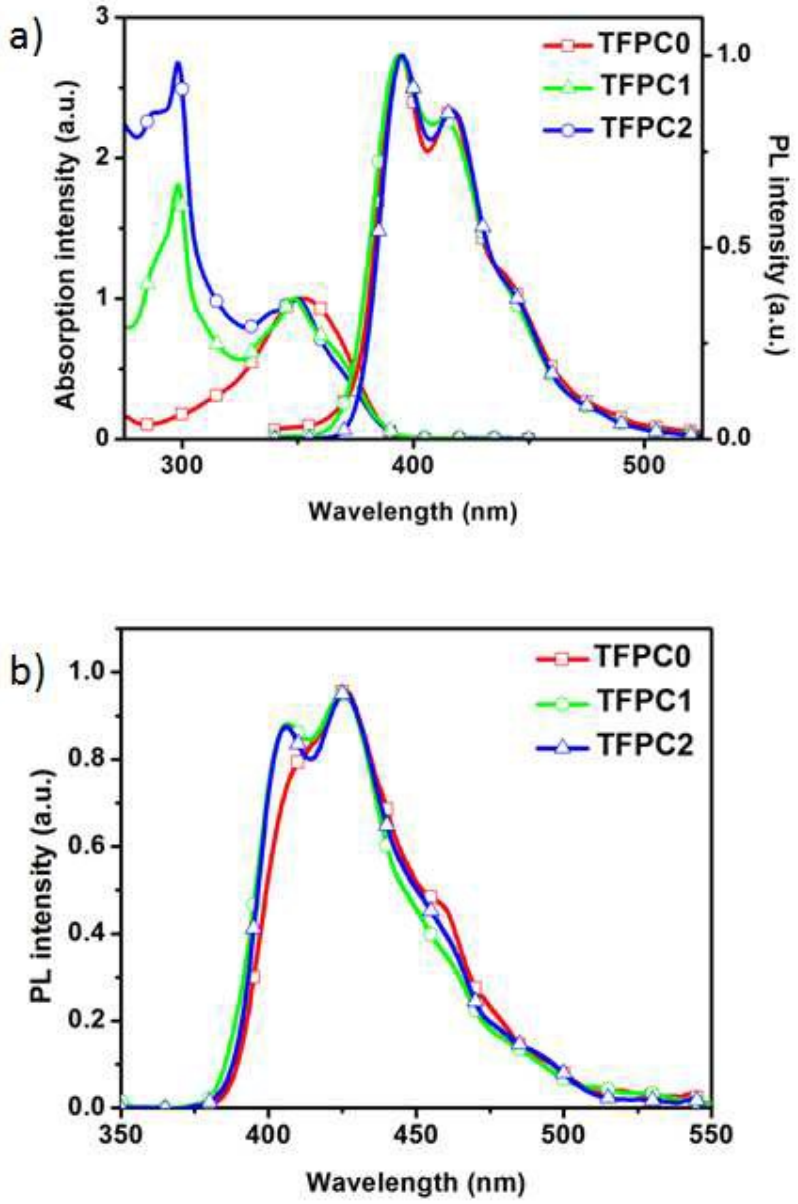

Figure 5. Absorption and PL spectra in toluene (10^{-6} M) (a) as well as PL spectra in film state (b) for TFPC0~TFPC2.

View Article Online
DOI: 10.1039/C5TC01711D

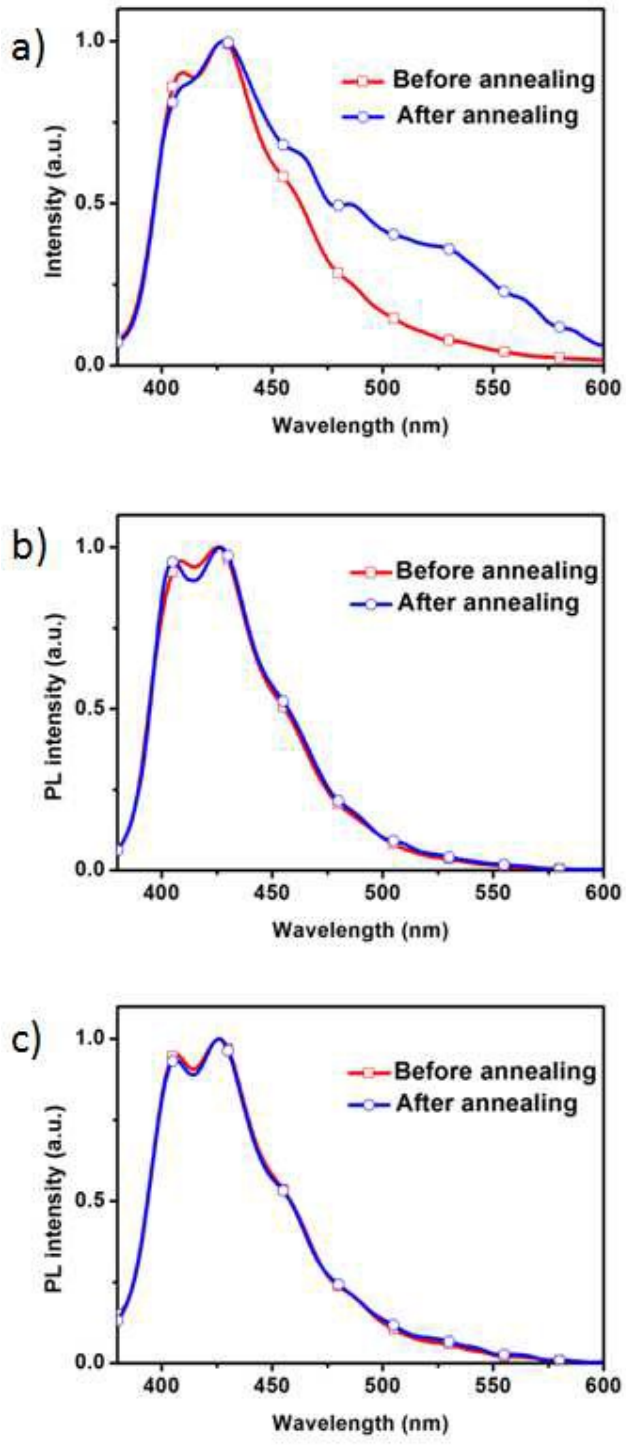

Figure 6. PL spectra of TFPC0 (a), TFPC1 (b) and TFPC2 (c) before and after annealling in air at 150 ^{o}C for 24 hours.

View Article Online
DOI: 10.1039/C5TC01711D

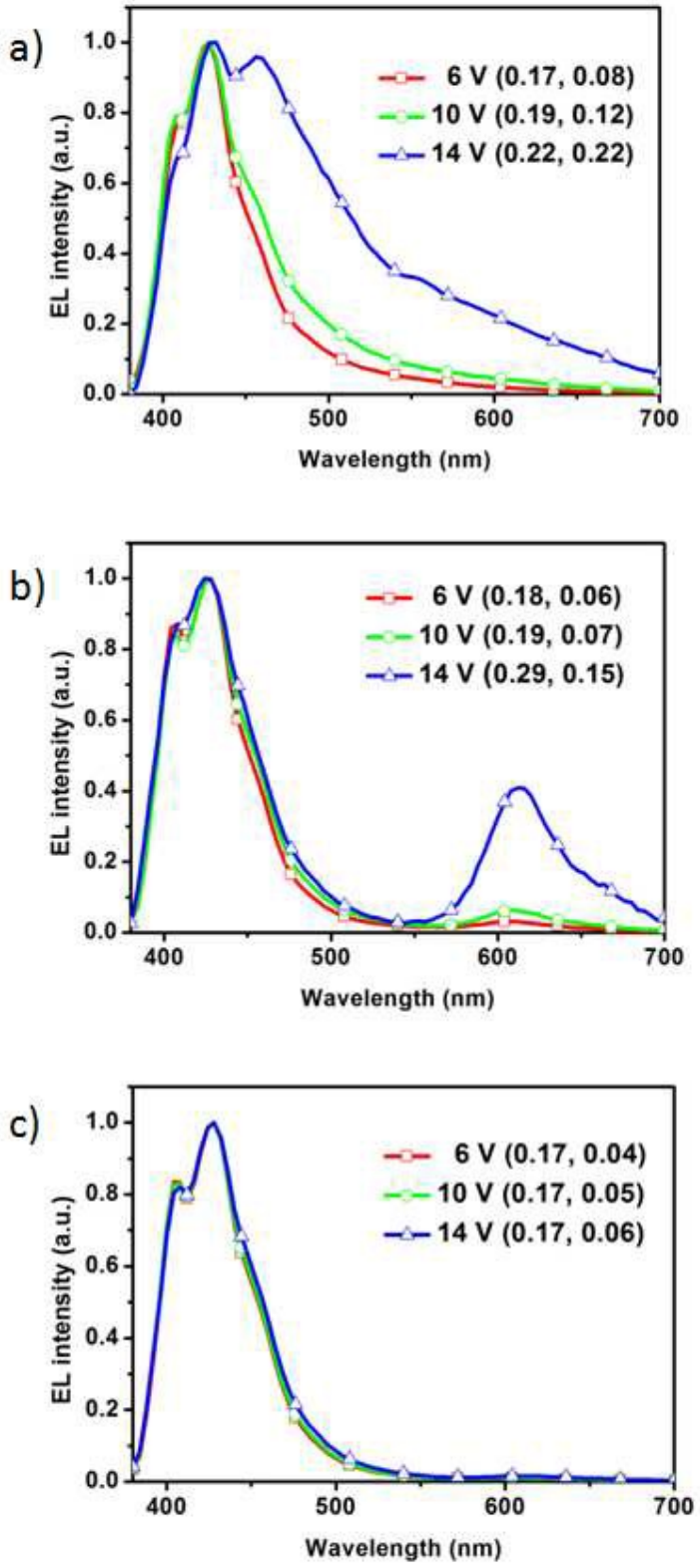

Figure 7. EL spectra of TFPC0 (a), TFPC1 (b) and TFPC2 (c) under different driving voltages for the single-layer devices.

View Article Online
DOI: 10.1039/C5TC01711D

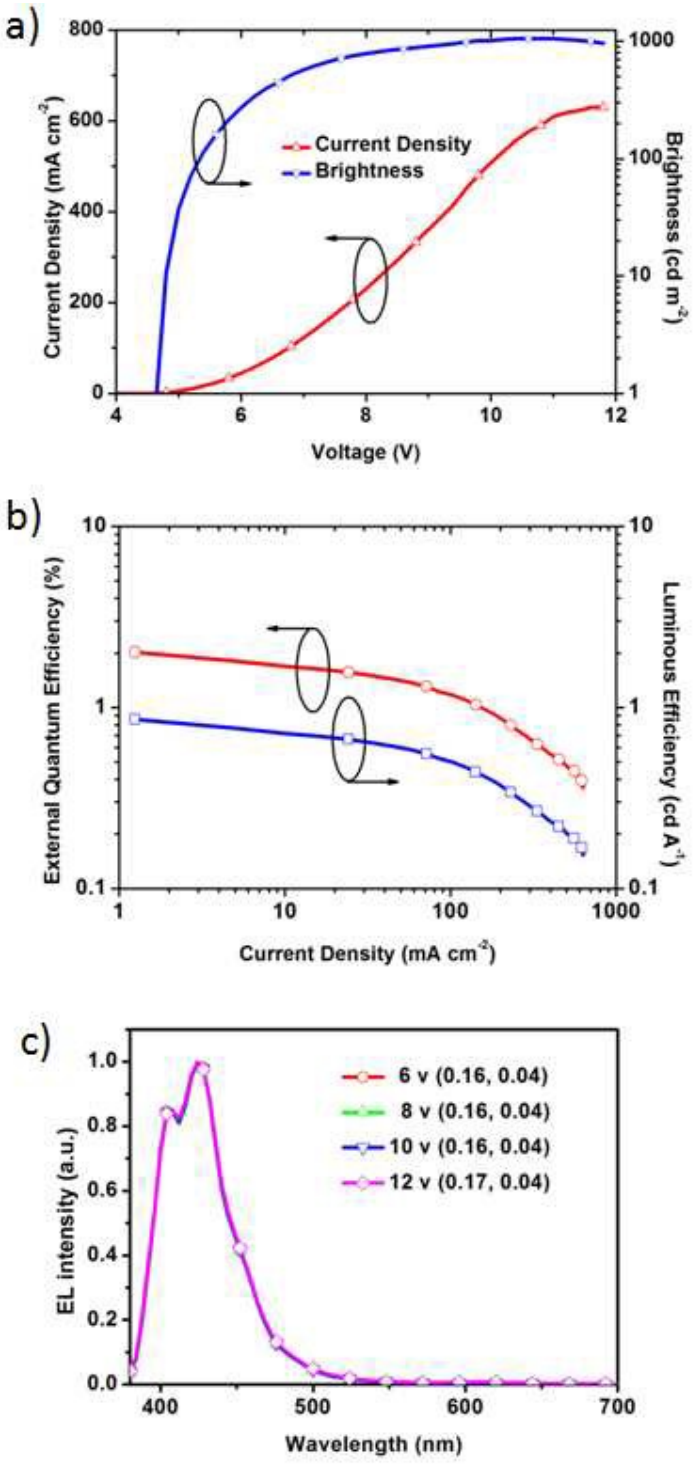

Figure 8. The current density-voltage-brightness characteristics (a), external quantum efficiency and luminous efficiency as a function of current density (b) as well as EL spectra at different driving voltages (c) for the double-layer device of TFPC2.

View Article Online
DOI: 10.1039/C5TC01711D

Table 1. Thermal, electrochemical and photophysical properties of TFPC0~TFPC2.

Compound	T_d [°C]	T_g/T_m [°C]	λ_{abs} [a] [nm]	λ_{em} [a] [nm]	τ [a] [ns]	Φ_{PL} [b] [%]	λ_{em} [c] [nm]	τ [c] [ns]	Φ_{PL} [d] [%]	HOMO [eV]	LUMO [eV]
TFPC0	471	190/374	352	395/417	0.78	88	413/426	0.33	39	-5.71	-2.52
TFPC1	503	304/n.d.	348/298	394/414	0.86	94	407/426	0.46	52	-5.52	-2.32
TFPC2	521	376/n.d.	349/298	395/417	1.60	69	406/426	0.50	36	-5.35	-2.15

[a] Measured in toluene at a concentration of 10^{-6} M. [b] Measured in toluene using 9,10-diphenylanthracene as a standard. [c] Measured in film. [d] Measured in film using an integrating sphere.

View Article Online
DOI: 10.1039/C5TC01711D

Table 2. EL performance of the devices.

Device	V_{on} [c] [V]	L_{max} [d] [cd m^{-2}]	$\eta_{c, max}$ [e] [cd A^{-1}]	$\eta_{p, max}$ [f] [lm W^{-1}]	$\eta_{ext, max}$ [g] [%]	CIE [h] (x, y)
TFPC0 [a]	5.6	178	0.07	0.03	0.08	(0.17, 0.08)
TFPC1 [a]	4.5	394	0.16	0.09	0.24	(0.18, 0.06)
TFPC2 [a]	5.3	183	0.05	0.02	0.11	(0.17, 0.04)
TFPC2 [b]	4.5	1054	0.86	0.56	2.02	(0.16, 0.04)

[a] ITO/PEDOT:PSS/EML/Ca/Al. [b] ITO/PEDOT:PSS/EML/TPBI/LiF/Al. [c] Turn-on Voltage. [d] Maximum luminance. [e] Maximum current efficiency. [f] Maximum power efficiency. [g] Maximum external quantum efficiency. [h] Commission Internationale de l'Eclairage coordinates at a driving voltage of 6 V.

View Article Online
DOI: 10.1039/C5TC01711D

View Article Online
DOI: 10.1039/C5TC01711D

Table of Contents

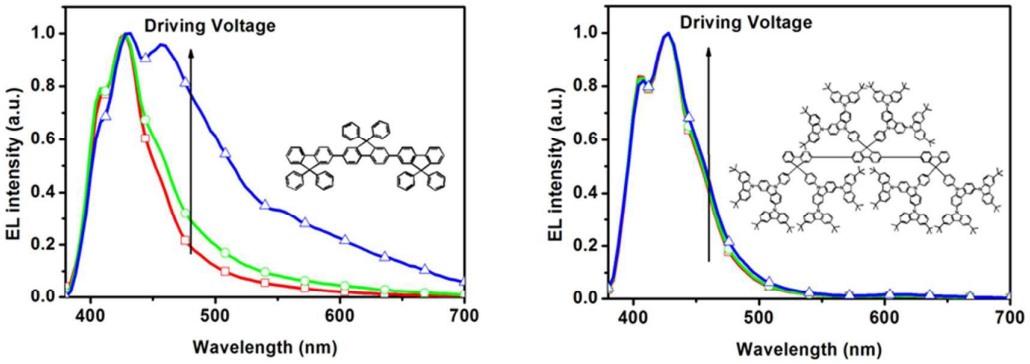

Deep-blue terfluorenes simultaneously with highly spectral stability and device efficiency have been successfully developed by functionalizing the backbone with carbazole dendrons, showing a peak external quantum efficiency as high as 2.02% and CIE coordinates of (0.16, 0.04) for solution-processed undoped OLEDs.